University of Nebraska - Lincoln
DigitalCommons@University of Nebraska - Lincoln

Faculty Publications: Materials Research Science and Engineering Center | Materials Research Science and Engineering Center

12-3-2003

Magnetic transitions in disordered $GdAl_2$

D. S. Williams
University of Nebraska - Lincoln

Paul M. Shand
University of Northern Iowa, paul.shand@uni.edu

Thomas M. Pekarek
University of Northern Florida, tpekarek@gw.unf.edu

Ralph Skomski
University of Nebraska-Lincoln, rskomski2@unl.edu

Valeri G. Petkov
Central Michigan University, petkov@phy.cmich.edu

See next page for additional authors

Follow this and additional works at: http://digitalcommons.unl.edu/mrsecfacpubs

Part of the Materials Science and Engineering Commons

Williams, D. S.; Shand, Paul M.; Pekarek, Thomas M.; Skomski, Ralph; Petkov, Valeri G.; and Leslie-Pelecky, Diandra, "Magnetic transitions in disordered $GdAl_2$" (2003). *Faculty Publications: Materials Research Science and Engineering Center.* Paper 14.
http://digitalcommons.unl.edu/mrsecfacpubs/14

This Article is brought to you for free and open access by the Materials Research Science and Engineering Center at DigitalCommons@University of Nebraska - Lincoln. It has been accepted for inclusion in Faculty Publications: Materials Research Science and Engineering Center by an authorized administrator of DigitalCommons@University of Nebraska - Lincoln.

Authors
D. S. Williams, Paul M. Shand, Thomas M. Pekarek, Ralph Skomski, Valeri G. Petkov, and Diandra Leslie-Pelecky

This article is available at DigitalCommons@University of Nebraska - Lincoln: http://digitalcommons.unl.edu/mrsecfacpubs/14

Magnetic transitions in disordered $GdAl_2$

D. S. Williams,[1] P. M. Shand,[2] T. M. Pekarek,[3] R. Skomski,[1] V. Petkov,[4] and D. L. Leslie-Pelecky[1]
[1]*Department of Physics and Astronomy and Center for Materials Research and Analysis, University of Nebraska–Lincoln, Lincoln, Nebraska 68588-0111, USA*
[2]*Department of Physics, University of Northern Iowa, 205 Physics Building, Cedar Falls, Iowa 50614, USA*
[3]*Department of Chemistry and Physics, University of North Florida, 4567 St. John's Bluff Road South, Jacksonville, Florida 32224, USA*
[4]*Department of Physics, Central Michigan University, 203 Dow Science, Mt. Pleasant, Michigan 48859, USA*
(Received 7 August 2003; published 3 December 2003)

The role of disorder in magnetic ordering transitions is investigated using mechanically milled $GdAl_2$. Crystalline $GdAl_2$ is a ferromagnet while amorphous $GdAl_2$ is a spin glass. Nanostructured $GdAl_2$ shows a paramagnetic-to-ferromagnetic transition and glassy behavior, with the temperature and magnitude of each transition dependent on the degree and type of disorder. Disorder is parametrized by a Gaussian distribution of Curie temperatures T_C with mean $\overline{T_C}$ and breadth ΔT_C. A nonzero coercivity is observed at temperatures more than 20 K above the highest T_C of any known Gd-Al phase; however, the coercivity *decreases* with decreasing temperature over the same temperature range where the $GdAl_2$ grains ferromagnetically order. Models for the anomalous coercivity behavior are proposed and evaluated for their ability to explain the origin of the low-temperature glassy magnetization peak.

DOI: 10.1103/PhysRevB.68.214404 PACS number(s): 75.75.+a, 75.50.Tt

I. INTRODUCTION

Disorder on length scales comparable to magnetic interaction lengths often produces interesting—but complex—magnetic behavior. The dramatic dependence of magnetic properties on disorder motivates the need to understand how structural and chemical disorder affect magnetic ordering.

$GdAl_2$ is an ideal system for such an investigation as the magnetic properties range from ferromagnetic to spin-glass-like depending on the degree of disorder.[1,2] Crystalline $GdAl_2$ has $MgCu_2$ fcc structure ($a = 0.7899$ nm), a Curie temperature T_C of 170 K, and a small intrinsic magnetocrystalline anisotropy.[3,4] Amorphous $GdAl_2$ thin films, on the other hand, exhibit classic spin-glass behavior—a peak in the zero-field-cooled (ZFC) susceptibility (at $T_p = 16$ K), irreversibility between ZFC and field-cooled (FC) susceptibilities, and evidence of spin-glass scaling.[5,6] Curie-Weiss behavior is observed in both crystalline and amorphous $GdAl_2$ above their respective transition temperatures.[7]

Disorder is introduced by mechanical milling, which is a high-energy deformation process that generates defect structures (dislocations and vacancies), atomic-scale chemical disorder, and elastic strain energy through the shearing actions of ball-powder collisions.[8] Mechanical milling is distinct from mechanical alloying in that the latter combines two initially separate components, whereas mechanical milling starts with an ordered alloy that is progressively *disordered*.

We have investigated the paramagnetic-to-ferromagnetic (PM-FM) transition in highly disordered $GdAl_2$ to obtain information about the nature of the transition and impact of the resulting ferromagnetic structure on the glassy phase. The PM-FM transition in milled $GdAl_2$ shifts to lower temperature, broadens, and diminishes in intensity with milling time. A peak in the ZFC magnetization and irreversibility between the FC and ZFC magnetizations are observed, even after very short milling times; however, the peak temperatures are between 40 and 60 K—much higher than the 16-K peak temperature observed in amorphous $GdAl_2$.[1,2,9] This peak could be due to a true spin-glass transition[2] or could be attributable to a blocking transition.[9]

II. EXPERIMENTAL PROCEDURE

Gadolinium chips (99.9% pure) and aluminum pellets (99.99% pure) were arc melted under an argon atmosphere. The resulting buttons were turned and the procedure repeated several times to ensure homogeneous mixing. The alloy was crushed, milled for 2 h in a tungsten-carbide vial under an argon atmosphere to produce a fine powder, and then annealed for 24 h at 800 °C under vacuum to remove milling-induced stress. X-ray diffraction confirmed that the resulting material was a crystalline, highly ordered alloy and showed no tungsten carbide or oxide contamination.

Initially crystalline powders were milled in a high-intensity SPEX mill. Fifteen-minute milling periods were alternated with 15-min rest periods to reduce heating. The vial was turned every 2 h to reduce clumping, and small amounts of powder were removed at various intervals for structural and magnetic measurements. All sample handling was performed in an Ar atmosphere to prevent oxidation.

Samples for measurement in a superconducting quantum interference device (SQUID) magnetometer were prepared in an argon atmosphere and sealed in paraffin-filled polyethylene bags to protect the samples from oxidation during transfer to the SQUID and to prevent the particles from rotating during measurement.

III. STRUCTURAL CHARACTERIZATION

X-ray powder diffraction shows that, after about 20 h, the grain size of mechanically milled $GdAl_2$ reaches a terminal size of 6 ± 2 nm. Additional milling produces no further grain refinement. No evidence of contamination from the milling materials is observed via energy-dispersive x rays or

 ©2003 The American Physical Society

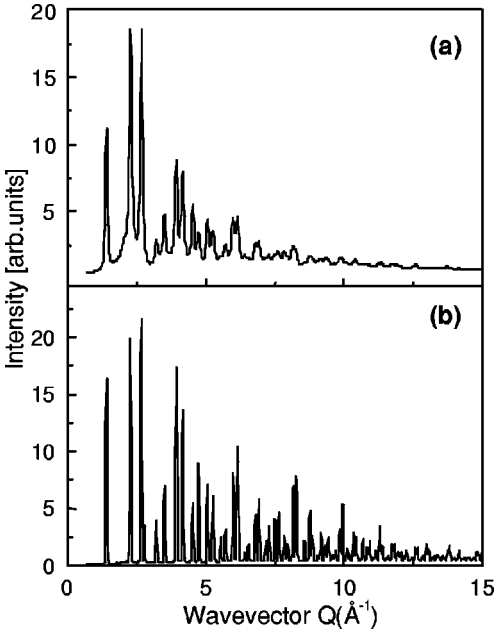

FIG. 1. Experimental powder diffraction patterns of (a) 400-h milled $GdAl_2$ and (b) unmilled (0-h) $GdAl_2$.

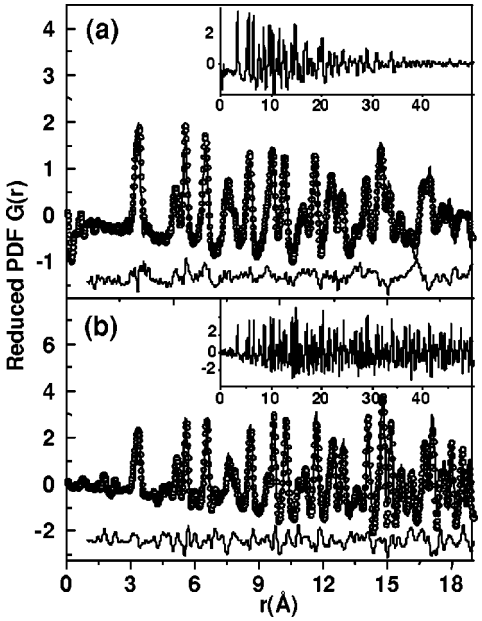

FIG. 2. Experimental (symbols) and model (solid line through the symbols) pair distribution functions for (a) 400-h milled $GdAl_2$ and (b) unmilled (0-h) $GdAl_2$. The residual differences between the experiments and models are shown as solid lines below each PDF. The insets show the PDF on an expanded scale in *q*.

x-ray diffraction, and samples milled for times up to 590 h and annealed at high temperatures do not show evidence of any non-Gd-Al phases.

High-energy x-ray diffraction experiments were performed at beamline 1-ID, SRI-CAT of the Advanced Photon Source, Argonne National Laboratory to probe the effect of longer-time milling. Samples milled for times up to 500 h were examined. Figure 1 compares the powder diffraction patterns of unmilled (alloyed, crushed, and annealed) $GdAl_2$ to the same material milled at a ball-to-powder ratio of 1:1 for 400 h. The diffraction pattern of unmilled $GdAl_2$ shows sharp Bragg peaks to wave vectors as high as 15 Å^{-1} as is typical in highly ordered crystalline materials. Bragg peaks in the diffraction pattern of the 400-h milled sample are significantly attenuated and merge into a slowly oscillating diffuse component by 10 Å.$^{-1}$

The diffraction patterns of highly disordered materials are difficult to analyze by traditional techniques; however, useful structural information may be obtained by analyzing the corresponding atomic pair distribution functions (PDFs).[10,11] The reduced PDF $G(r)=4\pi r[\rho(r)-\rho_0]$ is the Fourier sine transform of the elastic component of the powder diffraction data, where $\rho(r)$ and ρ_0 are the local and average atomic number densities, respectively. $G(r)$ peaks at characteristic distances separating pairs of atoms and thus describes the local structure of the material. Figure 2 shows the experimental PDFs obtained from the powder diffraction data of Fig. 1. Comparing the two PDFs emphasizes the dramatic reduction of the structural coherence with milling as demonstrated by the decay of the experimental PDF to zero (see the insets in Fig. 2). The milled sample has not lost its characteristic local atomic ordering since the experimental PDF can be reproduced by a nanocrystalline $GdAl_2$ model based on the $MgCu_2$-type structure with no evidence of amorphous or other crystallographically distinct phases.

The unit cell of $GdAl_2$ was fit to the experimental PDF data and the structure parameters (unit-cell constants and mean-squared atomic displacements) refined so as to obtain the best agreement between the model and experimental data. The fit was done using the program PDFFIT (Ref. 12) and was constrained to have the symmetry of the Fd3*m* space group. The best fit achieved is shown as a solid line through the datapoints in Fig. 2. The fit results show that after 400 h of milling, the lattice parameter of $GdAl_2$ is 0.7865(2) nm, which is a 0.45% decrease from the value measured in unmilled $GdAl_2$. The mean-squared atomic displacement factors are 0.0088(5) Å^2 for Gd (+193% relative to unmilled $GdAl_2$) and 0.0209(5) Å^2 for Al (+161% relative to unmilled $GdAl_2$).

Zhou and Bakker suggest that the disordering mechanism in mechanically milled $GdAl_2$ is a quadruple-defect disorder.[1] The difference in the sizes of Gd and Al atoms creates an inherent asymmetry: Al atoms can substitute in vacancies on the Gd sublattice, but not vice versa. This suggests that the grains are likely to be slightly Gd poor and the grain boundaries slightly Gd rich. We are left with a picture of long-time mechanically milled $GdAl_2$ as nanocrystalline on a length scale of 5 nm, but with numerous lattice defects and considerable local structural distortions.

IV. MAGNETIC PROPERTIES

The complex nanostructure of mechanically milled $GdAl_2$ results in a correspondingly complex magnetic picture. This section explores how the magnetic behavior in different temperature regimes leads to an overall picture of the impact of disorder on magnetic structure. In Sec. IV A, we will show

that the temperature dependence of the magnetization indicates the presence of a ferromagnetic phase (attributed to ordering within individual $GdAl_2$ grains) and a paramagnetic phase. Analysis of the PM-FM transition allows us to parametrize disorder in terms of a distribution of T_C's characterized by a mean Curie temperature $\overline{T_C}$ and an associated breadth ΔT_C. Section IV B focuses on hysteresis measurements that show an anomalous temperature dependence of the coercivity: an unexpected nonzero coercivity at the highest measured temperature of 315 K, followed by a decrease in coercivity as the temperature decreases over the temperature range where $GdAl_2$ grains ferromagnetically order. Finally, we will present two models in Sec. V that are consistent with these observations and then discuss whether these models are consistent with explanations for the low-temperature glassy transition.

A. Temperature dependence of the magnetization

A sample milled for 400 h at a ball-to-powder ratio of 1:1.75 was selected for an in-depth investigation of the magnetic properties because the PM-FM transition and the low-temperature peak are separated sufficiently in temperature to allow an independent investigation of each transition. Figure 3 shows M/H as a function of T in FC and ZFC configurations at fields from 5 to 5000 Oe for the 400-h milled $GdAl_2$ sample. Two distinct features are observed at low fields: a peak in the ZFC curve around 60 K and a shoulder near 130 K. The FC and ZFC curves split, with the temperature at which the split occurs decreasing with increasing field. No irreversibility is present in fields greater than 1000 Oe. The low-temperature peak shifts to lower temperatures with increasing field.

1. $T>T_C$: Curie-Weiss behavior

The high-temperature magnetization of unmilled $GdAl_2$ obeys a Curie-Weiss $[\chi=c/(T-\theta)]$ law with Curie constant $c=4.36(\pm 0.04)\times 10^{-2}$ emu K/g Oe and $\theta=171\pm 1$ K. The constant c is related to the effective moment by $N\mu_{\rm eff}^2=3c\mathcal{M}k_B$, where $\mathcal{M}$ is the molecular weight, k_B is the Boltzmann constant, and N is the number of atoms. The observed moment of $8.60(\pm 0.04)\mu_B$ is higher than the value of $7.9\mu_B$ expected from Gd^{3+} ions.[13] The excess moment observed in $GdAl_2$ usually is attributed to conduction-electron enhancement effects.[14]

Mechanically milled $GdAl_2$ cannot be described by a single Curie-Weiss expression. The best fit in the paramagnetic region ($T>170$ K) is given by Eq. (1), which is a combination of a Curie-Weiss term and a Curie term (a small constant-background term due to the phase that will be discussed in Sec. IV B was removed):

$$\chi(T)=\frac{c_1}{T-\theta}+\frac{c_2}{T}. \tag{1}$$

The value of θ for the 400-h milled sample is $137(\pm 2)$ K for fields up to 1 T. The Curie constants are $c_1=9.10(\pm 0.01)\times 10^{-3}$ emu K/g Oe and $c_2=3.42(\pm 0.06)\times 10^{-2}$ emu K/g Oe. Extracting the effective moments from the Curie-Weiss constants c_i is difficult because the fraction of the sample corresponding to each phase is not known. We find that $c_1<c_2$—i.e., $N_1(\mu_{\rm eff_1})^2<N_2(\mu_{\rm eff_2})^2$—for all milled samples. The effective moments of milled $GdAl_2$ are consistent with those of unmilled $GdAl_2$ in that the sum of c_1 and c_2 is comparable to the value of c for the unmilled material.[15] The high-temperature magnetization thus provides the first evidence that, although no secondary structural phases are found, the magnetic behavior cannot be explained by a single magnetic phase.

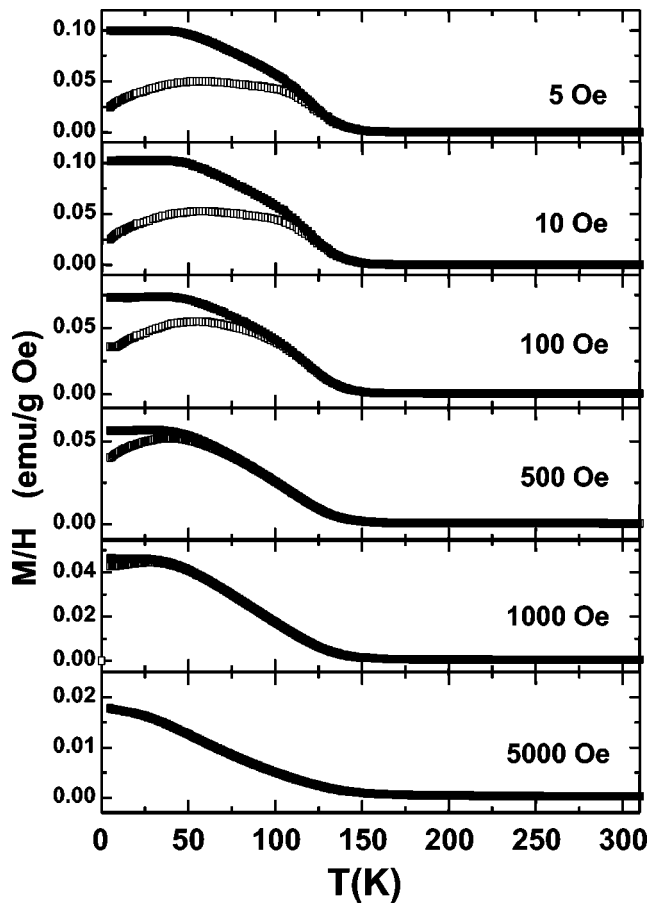

FIG. 3. Dependence of the magnetization divided by measuring field on temperature and field. The top curves in each graph are the field-cooled measurements and the lower curves are the zero-field-cooled measurements. No irreversibility is observed at fields above 1000 Oe.

2. Paramagnetic-ferromagnetic transition

Mechanically milled $GdAl_2$ has two types of inhomogeneity: the formation of grains interrupts the long-range coherence of the lattice, while disorder within the grains reflects inhomogeneity on the order of a few lattice spacings. As milling time increases, T_C decreases and the transition broadens. The transition temperature decrease is not due to grain-size reduction, as T_C changes little during the initial decrease in grain size, but changes significantly after the terminal grain size has been attained. As shown in Sec. III, the primary effect of long-time milling is to introduce atomic-

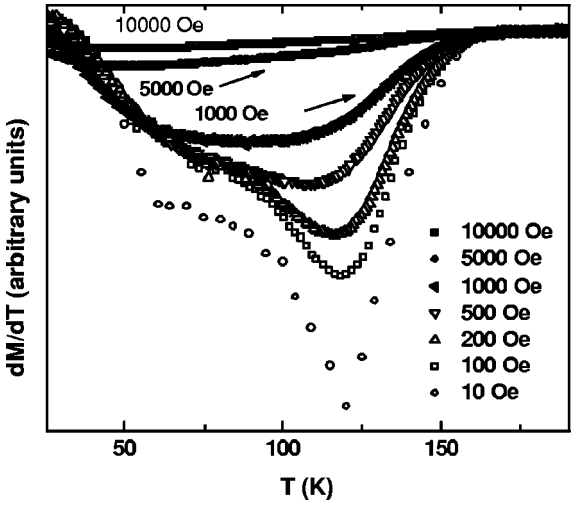

FIG. 4. $dM_{\mathrm{ZFC}}(T)/dT$ at measuring fields from 10 to 10 000 Oe.

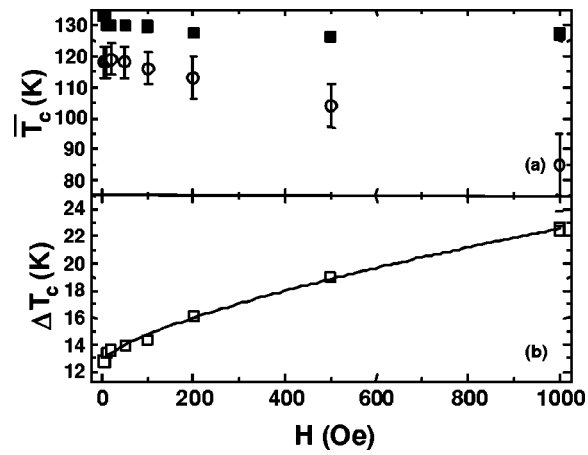

FIG. 5. (a) $\overline{T_C}$ and (b) T_C as functions of measuring field for the 400-h milled sample. The solid squares in (a) and the open squares in (b) are values from fitting to Eq. (2). The solid line in (b) is a fit to Eq. (4). The open circles are the minima from Fig. 4.

level disorder. Since T_C in bulk $GdAl_2$ decreases with sample purity,[3] it is reasonable to assume that disorder should have the same effect. Different degrees of disorder are produced in different $GdAl_2$ grains and longer milling times produce broader ranges of disorder.

The effect of disorder on the PM-FM transition can be quantified by considering the field dependence of the transition. The mean transition temperature $\overline{T_C}$ is often identified by the "kink point"—the temperature of the minimum in $dM(T)/dT$. The PM-FM transition in the 400-h milled sample broadens with field, as seen more clearly in the plot of dM/dT vs T in Fig. 4.

Substitutionally disordered materials such as $La_{2/3}Ca_{1/3}MnO_3$ and $La_{0.5}Sr_{0.5}CoO_3$ are inhomogeneous on the same length scale as the disordered $GdAl_2$ grains due to the intrinsic concentration variations of randomly doped mixed-valence states.[16–18] Berger *et al.*[17] modeled the magnetization of $La_{2/3}Ca_{1/3}MnO_3$ using

$$M(T)=m_0\int_{T_C}\left(\frac{T_C-T}{T_C}\right)^{\beta}\theta(T_C-T)\rho(T_C)dT_C, \qquad (2)$$

where $\theta(T_C-T)$ is the Heaviside step function, m_0 is proportional to the saturation magnetization, and $\rho(T_C)$ describes a Gaussian distribution of Curie temperatures with mean value $\overline{T_C}$ and breadth ΔT_C:

$$\rho(T_C)=\frac{1}{\sqrt{2\pi}\Delta T_C}e^{(T_C-\overline{T_C})^2/2(\Delta T_C)^2}. \qquad (3)$$

Equations (2) and (3) successfully describe $La_{2/3}Ca_{1/3}MnO_3$ films with exponents in agreement with the three-dimensional (3D) Heisenberg model.[17] While it is significant that this model can determine critical behavior in systems where the intrinsic broadening due to disorder is comparable to the field broadening, our primary interest is in using it as a means of quantifying disorder.

The magnetization as a function of temperature for the 400-h $GdAl_2$ sample near the PM-FM transition was fit to Eq. (2) at different magnetic fields. The range of temperatures used depends on the field, but typically includes data to about 20–25 K below $\overline{T_C}$. The parameters are not very sensitive to the range of the data included in the fit unless data from the region where the PM-FM transition starts to overlap the glassy transition are included. To avoid divergences in the fits due to the form of Eq. (2), the data are fit by fixing β and determining values for the other parameters, then changing β and refitting. The best fits are identified by the lowest reduced χ^2 for a given data set. Large uncertainties in β are obtained for fields greater than 1000 Oe. The inability to obtain satisfactory fits above $H=1000$ Oe may be due to the inapplicability of mean-field theory at high field and/or to the broadening of the PM-FM transition to a point where it overlaps the glassy transition. The exponent β plotted as a function of field extrapolates linearly to a value of $\beta(H=0)=0.52\pm0.05$, which is consistent with the value expected for a mean-field system.

The parameters $\overline{T_C}$ and ΔT_C are robust: their values change little over the range of uncertainty in β. Figure 5 shows the dependence of the parameters $\overline{T_C}$ and ΔT_C on magnetic field. Figure 5(a), which compares the values of $\overline{T_C}$ to the "kink point" values, shows that the kink point values are consistently lower than $\overline{T_C}$ and show more pronounced field dependence. $\overline{T_C}$ should depend on the (field-independent) degree of disorder in the material, so change with field is not expected. The discrepancy between the results of the two methods indicates that the minimum in $dM(T)/dT$ may not be a good estimate of T_C in inhomogeneous ferromagnets, especially if taken from measurements in a moderately large field. The Curie-Weiss temperature θ from the fit to Eq. (1) is comparable to $\overline{T_C}=128(\pm2)$ K from the fit to Eq. (2), showing that the phase responsible for the PM-FM transition is the same as the phase identified by the Curie-Weiss behavior. The distribution of T_C's is due to the different degrees of disorder in different $GdAl_2$ grains.

Berger *et al.*[17] found that the breadth of the T_C distribu-

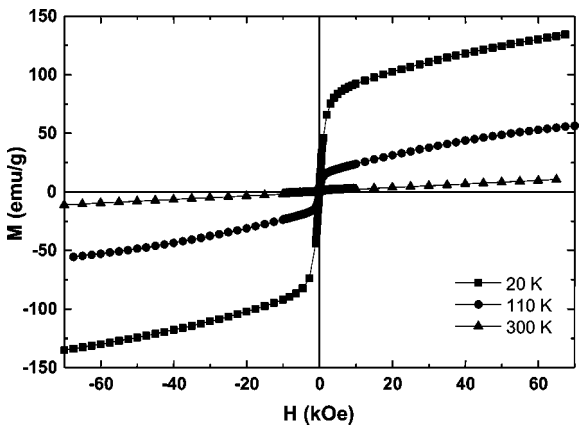

FIG. 6. $M(H)$ for temperatures of 300 K, 100 K, and 20 K.

tion in the inhomogeneous ferromagnet $La_{1/3}Ca_{1/3}MnO_3$ depends on field as

$$\Delta T_C(H)=\Delta T_C(H=0)+cH^{1/\eta}, \tag{4}$$

where $\Delta T_C(H=0)$ is an intrinsic breadth. The solid line in Fig. 5(b) is a fit to Eq. (4) with $\Delta T_C(H=0)=12.7$ (± 0.2) K and $\eta=1.45(\pm 0.15)$. This value of η is close to that obtained from calculations using a mean-field approximation ($\eta=1.50$), which is in turn consistent with the value of $\beta(H=0)=0.5$.

Mean-field values may be reasonable in a nanostructure: If the transitions measured are *within* the $GdAl_2$ grains, finite-size effects in ferromagnets are expected to be significant only at smaller length scales. Spins coupled by a long-range exchange interaction may also be characterized by mean-field exponents.

B. Hysteresis measurements

Hysteresis loops $M(H)$ for the 400-h milled sample were measured over a range of temperatures, with all measurements made after zero-field cooling. Figure 6 shows the upper branch of representative hysteresis loops for $T=300$, 110, and 20 K. Bulk $GdAl_2$ above T_C is purely paramagnetic with $\chi=2.6\times 10^{-4}$ emu/g Oe at 310 K and no hysteresis. In contrast, the hysteresis loops of the 400-h milled sample are a superposition of a hysteretic (h) and a nonhysteretic (nh) contribution at all temperatures. The nonhysteretic part is due to paramagnetic or superparamagnetic behavior and is modeled by a Langevin function, while the hysteresis is modeled by a phenomenological form[19] described by

$$M(H)=M_{nh}(H)+M_h(H)=m_0^{nh}L\left(\frac{n\mu_B H}{k_B T}\right)+m_0^h\frac{2}{\pi}\tan^{-1}\left[\left(\frac{H\pm H_C}{H_C}\right)\tan\left(\frac{\pi S}{2}\right)\right], \tag{5}$$

where $L(x)$ is the Langevin function, k_B is Boltzmann's constant, and H_C is the coercivity. $n\mu_B$ is thus an effective moment (or "superspin") and the m_0^i $(i=h,nh)$ are the saturation magnetizations. S, the squareness of the hysteresis loop, varies between 0 and 1 and describes the slope of the loop.

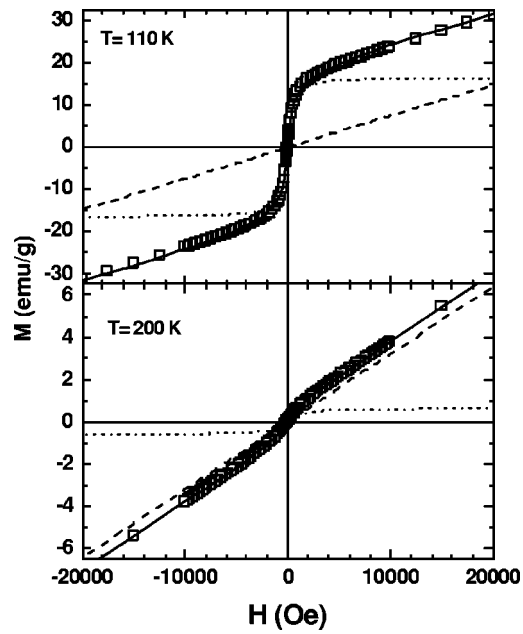

FIG. 7. The upper branch of the hysteresis loop taken at 110 K (top) and 200 K (bottom): Data are shown as squares, the contribution from the hysteretic component as a short dashed line, and the nonhysteretic contribution as longer dashes.

The hysteretic and nonhysteretic terms in Eq. (5) do not correspond to the same structural phases at all temperatures. For example, $GdAl_2$ grains are paramagnetic at their highest temperatures. This contribution and the contribution from the paramagnetic phase identified by the Curie-Weiss analysis both contribute to the nonhysteretic component. When the $GdAl_2$ grains begin to order, they will contribute a superparamagnetic component, in addition to the contribution from the Gd ions in the paramagnetic phase. When they fully order and begin to correlate with each other, they will contribute to the hysteretic term.

Figure 7 shows the separate contributions of the hysteretic and nonhysteretic terms for $T=200$ and 110 K. The values of H_C from the fit to Eq. (5) are shown in Fig. 8. The coercivity displays two unexpected behaviors: First, coercivity on the order of 60 Oe is observed from 200 to 315 K. Second, the coercivity value *decreases* as the temperature decreases from 170 to 130 K.

Above 250 K, the nonhysteretic contribution can be modeled as a simple paramagnetic background with $\chi\sim 1.5\times 10^{-4}$ emu/g Oe or as a Brillouin function with $j=7/2$; however, the magnetization does not saturate at the highest available field of 7 T, so differentiating between the two forms is impossible. As the temperature decreases, $M_{nh}(H)$ can no longer be represented by a constant paramagnetic susceptibility and requires the use of the Langevin. The values of n are larger than those expected for isolated Gd ions, suggesting cooperative behavior between Gd ions within the grains. The superposition of $M_{nh}(H)$ vs H/T at different temperatures would confirm superparamagnetic behavior; however, the dependence of n on temperature precludes the superposition. This situation is in contrast to isolated nanoparticle systems where the number of spins in spatially dis-

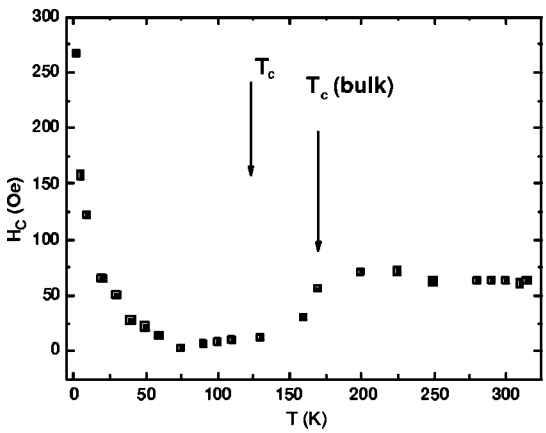

FIG. 8. The coercivity obtained from Eq. (5) as a function of temperature.

tinct groups remains constant with temperature. There is no significant change in the value of the saturation magnetization in the hysteretic term over this temperature range. The coercivity, however, exhibits a surprising decrease between 170 and 130 K: i.e., over the temperature range from the bulk T_C of $GdAl_2$ to the T_C for $GdAl_2$ grains in this specific sample (128 K). Below the T_C value of this sample, the coercivity increases, with no distinct features at the position of the peak in the ZFC magnetization.

V. DISCUSSION

The structural evidence indicates that mechanically milled $GdAl_2$ consists of 5–7-nm Gd-poor $GdAl_2$ grains with different degrees of chemical disorder. The excess Gd atoms presumably form a Gd-rich Gd-Al grain boundary phase. Curie-Weiss analysis and the fits to the data in the neighborhood of the PM-FM transition show ferromagnetic ordering over a range of temperatures, with a mean ordering temperature of 128 K. The hysteresis measurements, however, show that there is a nonzero coercivity well above the T_C of not only $GdAl_2$, but of any known Gd-Al phase. [Among ferromagnetic phases, Gd_3Al_2 has $T_C = 282$ K (Ref. 20) and Gd has $T_C = 293$ K (Ref. 13).] The coercivity exhibits an anomalous decrease coincident with the temperature range over which the $GdAl_2$ grains order.

We suggest that the high-temperature coercivity is due to the formation of small Gd or Gd-rich clusters in the grain boundaries. Gadolinium has partially filled $4f$ shells with a spherical ground-state charge distribution that cannot interact with the crystalline environment. The large spin-orbit coupling of the Gd $4f$ electrons thus does not translate into magnetocrystalline anisotropy.[21] There is, however, a significant magnetostatic contribution to the Gd anisotropy due to the large and stable Gd moment, which leads to pronounced dipolar interactions.

At $T=0$, the coercivity of an ensemble of N interacting Gd atoms can be written as $H_c = \alpha M_{Gd}$, where $M_{Gd} = 2.527\ T/\mu_0$ is the saturation magnetization of ferromagnetic Gd and α is a dimensionless but structure-dependent coercivity parameter. For clusters with cubic symmetry, $\alpha = 0$, whereas for a pair of ferromagnetically coupled Gd atoms a distance R apart,

$$\alpha = \frac{3}{\pi\sqrt{2}} \frac{R_{Ga}^3}{R^3}, \tag{6}$$

where $R_{Gd} = 1.787$ Å is the atomic radius of Gd. As a rule, α reflects the asphericity of the cluster and is weakly N dependent. This calculation is based on Néel's model,[22] which is exact for dipolar interactions.[23] Since $R \geqslant 2R_{Gd}$, Eq. (6) predicts a maximum coercivity of $(3/8\pi\sqrt{2})M_{Gd}$—i.e., 0.213 T. The unknown structure of the clusters makes it difficult to predict α for a given experimental system, but the value implied by Eq. (6) may serve as an upper bound.

Experimentally, Gd cluster-beam measurements find Curie temperatures significantly higher than the bulk T_C of Gd (T_C's of up to 800 K are reported),[24–26] and measurements of small Co clusters on surfaces[27] show that asymmetry-induced surface anisotropies can be significant. Inert-gas-condensed Gd compacts with grain sizes on the order of 5–10 nm also have a coercivity of the same magnitude as measured in these $GdAl_2$ nanostructures.[28] The argument for the presence of Gd-rich clusters is further strengthened by the observation that annealing a sample milled for 590 h results in a material with nanocrystalline $GdAl_2$ *and* Gd_2Al phases. Clustering of Gd may encourage the formation of the Gd_2Al phase. It is important to emphasize that physical Gd clusters are not required: the same phenomenon could occur in Gd-rich Gd-Al clusters (which means that detecting them via transmission electron microscopy would be unlikely).

Figure 9(a) schematically illustrates the high-temperature structure of mechanically milled $GdAl_2$. Paramagnetic $GdAl_2$ grains (gray diagonally shaded areas) and Gd or Gd-rich Gd-Al clusters in the grain boundaries (white circles with black arrows) are in a Gd-Al grain boundary region (gray). The paramagnetic $GdAl_2$ grains become superparamagnetic as the temperature decreases and the $GdAl_2$ grains order. The $1/T$ dependence in Eq. (1) likely originates from the grain boundary, either due to simple paramagnetism or disorder that produces ferromagnetic and antiferromagnetic interactions balanced such that the behavior approximates a Curie law.

Some fraction of the $GdAl_2$ grains are ferromagnetically ordered at an arbitrary temperature between 130 and 170 K, with the number of ordered grains depending on the temperature and the amount of disorder in each grain [Fig. 9(b)]. Although the majority of the coercivity decrease occurs between 170 and 150 K, the system does not reach its lowest coercivity until 75 K, suggesting that ordering of the $GdAl_2$ grains occurs over a very broad temperature range. Hysteresis loop fits in this temperature range are of noticeably lower quality than those in the temperature regimes above and below: even fits to two Langevins and a hysteretic term fail to fit in the low-field region. It is likely that a distribution of H_C values is necessary for a satisfactory fit due to the range of disorder implied by the T_C distribution; however, this procedure results in an unreasonably large number of fitting parameters.

We will examine two models that explain the decrease in

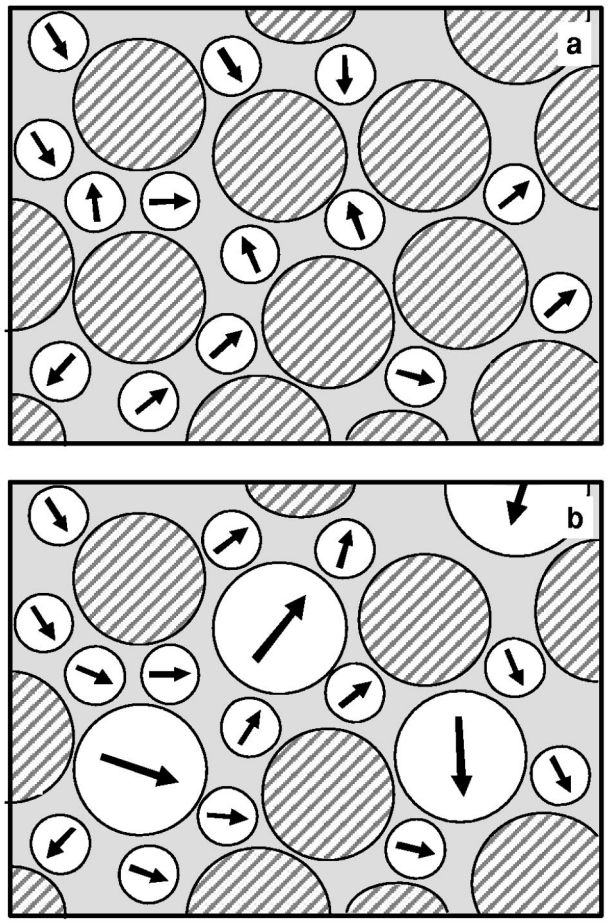

FIG. 9. Schematic illustration of the magnetic structure of mechanically milled $GdAl_2$. (a) At $T>170$ K, the structure is composed of paramagnetic $GdAl_2$ grains (gray diagonal shaded areas), ferromagnetically aligned Gd-rich clusters in the grain boundaries (white circles with black arrows), and a Gd-Al grain boundary (gray). (b) below $T\sim170$ K, $GdAl_2$ grains start to order (large white circles with arrows), although not all of the grains order at the same temperature.

the coercivity and discuss the impact of each on the possible origins of the low-temperature glassy peak. The first possibility is that exchange coupling between ordered $GdAl_2$ grains and Gd clusters overcomes the independent behavior of the Gd clusters and produces superparamagnetic entities that have reduced coercivity. This model implies that hysteresis loops in this temperature range should be modeled by two Langevin terms; however, the coercivity does not drop entirely to zero over most of the range, so a hysteretic contribution is required. Since the superparamagnetic entities are likely to interact, even at these temperatures, a model of just two Langevin terms is not likely to be realized.

The second model is that the FM-ordering $GdAl_2$ grains magnetically couple the Gd clusters and the coercivity decreases due to the same type of anisotropy averaging as in a random anisotropy system.[29,30] The locally ordered regions may or may not percolate throughout the sample at a given temperature. Aeppli *et al.*[31] suggest a model for reentrant spin glasses that partitions the system into spin-glass-like and ferromagnetic subnetworks, which could be coupled or act independently. If the FM phase freezes first (as in our case), a system with coupled subnetworks will have a higher spin-glass freezing temperature than the uncoupled subnetwork case, where the two transitions occur independently of each other. Although this model was developed for amorphous materials, it could also apply to nanostructures, where the locally ferromagnetically aligned regions are defined by the $GdAl_2$ grains. The spin-glass behavior could arise from the grain boundary phase or it could be due to isolated grains that are not coupled to the ferromagnetic backbone and behave like a spin glass.

In model 2, ferromagnetic order extends across multiple grains upon passing through the PM-FM transition, while FM ordering is restricted to localized regions in model 1. In the first model, the glassy behavior would most likely be due to freezing of the superparamagnetic regions with respect to each other, while the second model attributes the glassy transition to a distinct phase (which may or may not be coupled to the FM network).

In the first model, the PM-FM transition is an integral part of explaining the low-temperature behavior; however, Zhou and Bakker[2] have produced samples showing a peak in the ZFC magnetization, but without obvious evidence of a PM-FM transition. Zhou and Bakker argue that superexchange between Gd atoms—mediated by the *p* character of Al—produces the competing antiferromagnetic and ferromagnetic interactions required for a spin glass. The implication of this argument is that spin-glass behavior is an *intrinsic* property of chemically disordered $GdAl_2$. Zhou and Bakker's argument is consistent with model 2: Milling converts the two-subnetwork ferromagnetic/spin glass system into an single-phase spin glass.

The first model, in contrast, identifies the glassy phase as being an *extrinsic* property of the sample, as the glassy transition is preceded by ordering *within* grains. This possibility is not excluded entirely by Zhou and Bakker's measurements. The sample they studied that showed no obvious PM-FM transition has larger grains ($\sim$20 nm) and more disorder (smaller lattice parameter), than our sample, in which grains are smaller and—on average—less disordered, with a larger fraction of sample being grain boundary. It is possible that a very large ΔT_C (due to a larger range of disorder) in Zhou and Bakker's samples smears the PM-FM transition such that it is not detected. Their measurements show a very long high-temperature tail in $M(T)$ that may indicate the onset of short-range FM order over a broad range of temperatures. It is doubtful that milling an initially crystalline material entirely eliminates short-range chemical order. Since FM-ordered regions on the scale of a few nanometers have been suggested as a factor in the glassy transition in amorphous $GdAl_2$, it is conceivable that the remnants of ordered material in nanostructured $GdAl_2$ produce glassy behavior.[32] If this is the case, the details of the behavior would be much more dependent on the nanostructure of the sample and not just on the spin-glass-like phase. It is clear from this discussion that the current data cannot distinguish between the two models and that understanding the nature of the FM phase is critical to determining the origin of the low-temperature peak.

VI. CONCLUSIONS

Mechanically milled $GdAl_2$ has been used to investigate the effect of structural and chemical disorder on the PM-FM transition. Milling-induced disorder is modeled by a distribution of Curie temperatures parametrized by a mean Curie Temperature $\overline{T_C}$ and a distribution breadth ΔT_C. Analysis of the PM-FM transition shows that the ''kink-point'' method of identifying T_C can produce misleading results due to field-broadening effects. The observation of nonzero coercivity at temperatures up to 20 K higher than the T_C of any known Gd-Al phases is explained by the presence of small Gd or Gd-rich Gd-Al clusters in the grain boundaries that are ferromagnetically ordered due to surface anisotropy.

Two models have been proposed to explain the subsequent decrease in coercivity as the $GdAl_2$ grains ferromagnetically order, and the implications for the origin of the glassy transition are discussed. The primary difference between the models lies in that model 2 attributes the glassy behavior to the *intrinsic* properties of chemically disordered $GdAl_2$, while model 1 attributes them to *extrinsic* properties determined by the nanostructure. Our discussion of these models shows that investigating glassy transition by itself is not sufficient: the process by which the glassy system is achieved is key to understanding the mechanism for the low-temperature peak.

ACKNOWLEDGMENTS

The authors acknowledge helpful discussions with A.F. Hebard, R.C. Hilborn, R.D. Kirby, and J. Shield and experimental assistance from S.D. Shastri at the Advanced Photon Source. A.P.S. is supported by the DOE under Contract No. W-31-109-Eng-38. The authors acknowledge support from NSF Grant No. DMR 9875425 (D.L.-P.), Grant No. DMR 9975887 (T.M.P.), and the NSF MRSEC Program (Grant No. DMR-0213808).

[1] G. F. Zhou and H. Bakker, Phys. Rev. B **52**, 9437 (1995).
[2] G. F. Zhou and H. Bakker, Phys. Rev. Lett. **73**, 344 (1994).
[3] R. Kirchmayr and C. A. Poldy, in *Handbook on the Physics and Chemistry of Rare Earths*, edited by J. K. A. Gschneider, Jr. and L. Eyring (North-Holland, Amsterdam, 1979), p. 55.
[4] E. M. Levin, V. K. Pecharsky, and K. A. Gschneidner, J. Appl. Phys. **90**, 6255 (2001).
[5] A. P. Malozemoff and J. P. Jamet, Phys. Rev. Lett. **39**, 1293 (1977).
[6] B. Barbara, A. P. Malozemoff, and Y. Imry, Phys. Rev. Lett. **47**, 1852 (1981).
[7] T. Mizoguchi, T. R. McGuire, S. Kirkpatrick, and R. J. Gambino, Phys. Rev. Lett. **38**, 89 (1977).
[8] C. C. Koch, Annu. Rev. Mater. Sci. **19**, 121 (1989).
[9] L. Klein, Phys. Rev. Lett. **74**, 618 (1995).
[10] T. Proffen, V. Petkov, S. J. L. Billinge, and T. Vogt, Z. Kristallogr. **217**, 47 (2002).
[11] V. Petkov, S. J. L. Billinge, P. Larson, S. D. Mahanti, T. Vogt, K. K. Rangan, and M. G. Kanatzidis, Phys. Rev. B **65**, 092105 (2002).
[12] T. Proffen and S. J. L. Billinge, J. Appl. Crystallogr. **32**, 572 (1999).
[13] K. A. McEwen, in *Handbook on the Physics and Chemistry of the Rare Earths*, edited by K. A. Gschneidner, Jr. and L. Eyring (North-Holland, Amsterdam, 1978), Vol. 1, p. 411.
[14] M. Bauer, M. S. S. Brooks, and E. Dormann, Phys. Rev. B **48**, 1014 (1993).
[15] D. Williams, P. M. Shand, C. Stark, T. Pekarek, R. Brown, L. Yue, and D. L. Leslie-Pelecky, J. Appl. Phys. **93**, 6525 (2003).
[16] D. N. H. Nam, K. Jonason, P. Nordblad, N. V. Khiem, and N. X. Phuc, Phys. Rev. B **59**, 4189 (1999).
[17] A. Berger, G. Campillo, P. Vivas, J. E. Pearson, S. D. Bader, E. Baca, and P. Prieto, J. Appl. Phys. **91**, 8393 (2002).
[18] X. G. Li, X. J. Fan, G. Ji, W. B. Wu, K. H. Wong, C. L. Choy, and H. C. Ku, J. Appl. Phys. **85**, 1663 (1999).
[19] M. B. Stearns and Y. D. Cheng, J. Appl. Phys. **75**, 6894 (1994).
[20] W. E. Wallace, *Rare Earth Intermetallics* (Academic, New York, 1973).
[21] R. Skomski and J. M. D. Coey, *Permanent Magnetism* (Institute of Physics, Bristol, 1999).
[22] L. Néel, J. Phys. Radium **15**, 225 (1954).
[23] Y. Millev, R. Skomski, and J. Kirschner, Phys. Rev. B **58**, 6305 (1998).
[24] D. C. Douglass, J. P. Bucher, and L. A. Bloomfield, Phys. Rev. Lett. **68**, 1774 (1992).
[25] D. C. Douglass, A. J. Cox, J. P. Bucher, and L. A. Bloomfield, Phys. Rev. B **47**, 12874 (1993).
[26] D. Gerion, A. Hirt, and A. Chatelain, Phys. Rev. Lett. **83**, 532 (1999).
[27] P. Gambardella, S. Rusponi, M. Veronese, S. S. Dhesi, C. Grazioli, A. Dallmeyer, I. Cabria, R. Zeller, P. H. Dederichs, K. Kern, C. Carbone, and H. Brune, Science **300**, 1130 (2003).
[28] D. Schmitter (unpublished).
[29] R. Alben, J. J. Becker, and M. C. Chi, J. Appl. Phys. **49**, 1653 (1978).
[30] G. Herzer, Mater. Sci. Eng., A **133**, 1 (1991).
[31] G. Aeppli, S. M. Shapiro, R. J. Birgeneau, and H. S. Chen, Phys. Rev. B **28**, 5160 (1984).
[32] S. C. Hart, P. E. Wigen, and A. P. Malozemoff, J. Appl. Phys. **50**, 1620 (1979).